

MAMBO image of the debris disk around ϵ Eridani : robustness of the azimuthal structure

Jean-François Lestrade¹ and Elodie Thilliez²

¹ Observatoire de Paris - LERMA, CNRS, 61 Av. de l'Observatoire, F-75014, Paris, France

² Centre for Astrophysics & Supercomputing, Swinburne University of Technology, Hawthorn, VIC, 3122, Australia

Received 27 November 2014 ; accepted 19 February 2015

ABSTRACT

The debris disk closest to Earth is the one around the star ϵ Eridani at a distance of 3.2 pc. It is the prime target for detailed studies of a belt of planetesimals left from the early phase of planet formation other than the Kuiper Belt. The non-uniform ring-like structure around ϵ Eridani, originally discovered at $\lambda = 850 \mu\text{m}$ with the bolometer camera *SCUBA*, could be the signpost of unseen long-period planets interior to the disk that gravitationally interact with it through mean-motion resonances. However, the reliability of the structure at $850 \mu\text{m}$, which has been debated, has not been verified with independent observations until now. We present a high signal-to-noise ratio image of this structure at $\lambda = 1.2 \text{ mm}$ made with the bolometer camera *MAMBO* and compare this with the *SCUBA* image. We have found that three of the four emission clumps (NE, NW, SW) and the two deep hollows to the east and west are at the same positions in the *MAMBO* and *SCUBA* images within astrometric uncertainty. The SE clump is at odds, significantly brighter and more extended in the *SCUBA* than in the *MAMBO* images, but it is possible that this mismatch is an artifact. We conclude that this degree of positional coincidence provides tentative evidence that the observed structure is robust. In addition, we present the radial brightness profile of our *MAMBO* image and show that the width of the planetesimal belt around ϵ Eridani is narrower than 22 AU, a more stringent upper limit than determined from previous observations. The corresponding relative width is $0.1 \leq \Delta R/R \leq 0.4$, which is lower than for the Kuiper Belt.

Key words. debris disks : circumstellar matter - planetary systems : formation - stars: planetary systems

1. Introduction

A debris disk is a constituting part of a planetary system according to the theory of formation and evolution of stars and planets. It is the analog of our asteroid belt, or Kuiper Belt. Such a belt is formed by the planetesimals that could not be turned into planets through agglomeration processes at work during the early formation phase. Although these remnant planetesimals are not directly observable when they surround other stars, their ongoing erosion through mutual collisions may generate enough dust to be detectable in thermal emission from mid-infrared to millimeter wavelengths or in scattered light (Wyatt 2008; Matthews et al. 2014).

The properties of such a belt – the radius, width, sharpness of edges, as well as radial and azimuthal structures – provide invaluable insights into possible perturbers, such as unseen planets just interior to the inner edge that cannot be detected by the radial velocity technique because they have very long orbital periods. Stars exterior to the system are likewise perturber candidates when the central star is part of a multiple system or is still embedded in the open cluster of its birth during the first one hundred Myr of its lifetime.

The debris disk closest to Earth known today is the one around ϵ Eridani, a mature K2 type star ($0.82 M_{\odot}$ in mass and $\sim 850 \text{ Myr}$ in age) that is only at 3.2 pc, ranked the tenth star in distance from the Sun.

A Jupiter-mass planet might orbit at about 3 AU from ϵ Eridani according to radial velocity and astrometric measurements (Hatzes et al. 2000; Benedict et al. 2006; Anglada-Escudé & Butler 2012), but a definitive interpretation of the measurements such as a seven-year orbital period of this companion, is complicated by stellar activity cycles (Cumming et al. 1999; Metcalfe et al. 2013).

The cold debris disk around ϵ Eridani was initially discovered with the *Infrared Astronomical Satellite (IRAS)* (Gillett 1986; Aumann 1988) and was later imaged at $850 \mu\text{m}$ and $450 \mu\text{m}$ in using the *James Clerk Maxwell telescope (JCMT)* with the *Submillimeter Common-User Bolometer Array (SCUBA)* (Greaves et al. 1998, 2005). These images showed a ring similar to our Kuiper Belt with a noticeably azimuthal structure. The disk is observed almost face-on and offers a unique opportunity for detailed studies.

Short-wavelength observations of a debris disk predominantly trace emission of fine grains that are dynamically scattered by radiation or stellar wind forces; these observations yield smooth images. In contrast, millimeter-wave observations predominantly trace millimeter-sized particles whose spatial distribution is controlled by mutual collisions and gravity, not by pressure radiation (Wyatt et al. 1999; Augereau & Beust 2006; Thebault et al. 2014; Kral et al. 2014). Images at long-wavelength are usually more structured than at short-wavelengths, and the presence of clumps has been related to dynamical perturbations of unseen planets.

Send offprint requests to: J-F Lestrade, e-mail: jean-francois.lestrade@obspm.fr

In this paper, we present a high signal-to-noise ratio image of the structure around ϵ Eridani at 1.2mm acquired with the 117-channel Max-Planck Bolometer array *MAMBO-2* at the *Institut de Radioastronomie Millimétrique (IRAM)* 30-meter telescope on Pico Veleta in Spain. The broad characteristics of the structures found in this new image at 1.2 mm corroborate the azimuthal structure previously identified in the 850 μ m image made with *SCUBA/JCMT* at a similar sensitivity. In addition, the width of the ring-like structure appears unresolved with the beam of the *IRAM* 30-meter telescope (10.7''), which is smaller than the *JCMT* beam.

In Sect. 2, the observations conducted with *MAMBO-2* are presented. In Sect. 3, the total flux density of ϵ Eridani measured at 1.2mm is used to study the Rayleigh-Jeans tail of the spectral energy distribution (SED). In Sect. 4, the *MAMBO* and *SCUBA* images and their azimuthal profiles are compared. In Sect. 5, the radial brightness profile from our *MAMBO* image is shown to be unresolved with the 10.7'' FWHM beam of the *IRAM* 30-meter telescope. In Sect. 6, we argue that kinship between the *MAMBO* and *SCUBA* images provides tentative evidence that the emission clumps of the structure are real.

2. MAMBO observations

We mapped the field around ϵ Eridani with the 117-channel Max-Planck Bolometer array *MAMBO-2* (Kreysa et al. 1998) of the *IRAM* 30-meter radiotelescope on Pico Veleta, Spain (2900 m). *MAMBO-2* has a half-power spectral bandwidth from 210 to 290 GHz, with an effective frequency centered on 250 GHz (1.20 mm) for thermal emission spectra. The 117-channel array is 240'' \times 240'' in size, and the bolometers are arranged in a hexagonal pattern with a beam separation of 22''. This is twice the effective FWHM beam (10.7'') and provides an undersampled image.

We used the standard on-the-fly mapping technique, where one map consists of 39 azimuthal subscans of 74 sec in duration each with a scanning velocity of 5''/sec over 370'' in azimuth, and with an incremental step of 8'' over 312'' in elevation, while wobbling the secondary mirror at 2 Hz by 60'' or 46'' in azimuth (the observations are split between the two throws). This scanning pattern produces time streams of data that are converted into a fully sampled spatial map with 3.5'' pixels.

We conducted 14 forty-eight-minute observations of the field around ϵ Eridani on nine different days between November 16 and December 4, 2007, totaling 11.2 hours of on-source observations. Atmospheric conditions were good during these winter observations, with typical zenith opacities between 0.1 and 0.3 at 250 GHz and low sky noise, that is, low atmospheric fluctuations. The telescope pointing was checked before and after each forty-eight-minute map by using the same nearest bright point source (J0339-018); it was found to be stable to greater accuracy than 3''. The absolute flux calibration is based on observations of several standard calibration sources, including planets, and on a tipping curve (sky dip) of the atmospheric opacity once every few hours. The resulting absolute flux calibration uncertainty is estimated to be about 10% (rms).

The data were analyzed using the mopsic software package written by R. Zylka at *IRAM*. The chopped observations acquired with the telescope pointing alternately on and off source at the wobbler rate produce double-beam

maps that were combined to a single map using the shift-and-add procedure¹ (Emerson et al. 1979). Compared to a complete image restoration, this produces maps with a sensitivity higher by about a factor 2, at the expense of no sensitivity to emission structures in scan direction that are larger than the wobbler throw of 60'' or 46''. The intensity map of the entire field observed around ϵ Eridani is presented in Fig 1. The total integration time of 11.2 hours yielded an rms noise of ~ 0.81 mJy/11'' beam in the central part of the co-added map ($r < 50''$) where the structure is located. As seen in Fig 1, noise is not uniform across the map because the scanned field is about twice as large as the bolometer array size, so that more data are taken in the central region of the map, where the source of interest is, than near the edges.

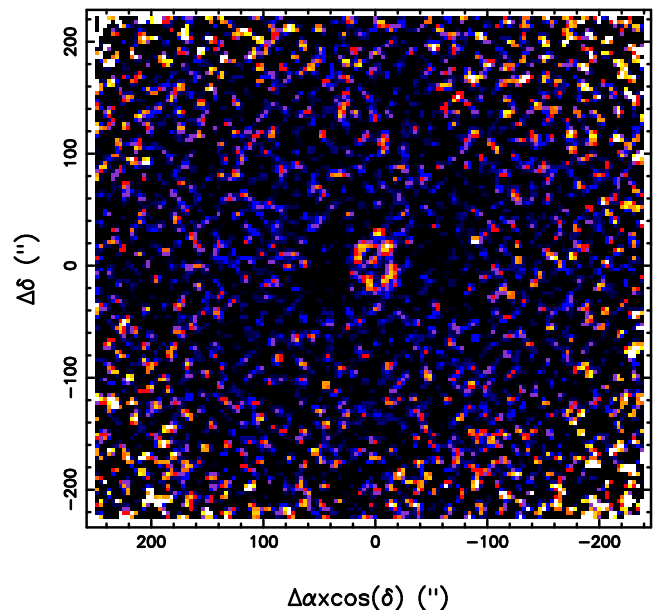


Fig. 1. Intensity map of the entire field around ϵ Eridani observed at $\lambda = 1.2$ mm with *MAMBO* in November 2007 at Pico Veleta (*IRAM* 30-meter radiotelescope). A ring is clearly apparent in the central region of the map centered on the position of ϵ Eridani on 15 November 2007 ($\alpha = 3^{\text{h}} 32^{\text{m}} 55.32^{\text{s}}$ and $\delta = -9^{\circ} 27' 29.7''$). The point source interior to the ring is within one pixel from the map center coincidental with the photosphere of ϵ Eridani. Within 50'' from the map center, the noise rms is 0.81 mJy/11'' beam, and the peak brightness is 3.1 mJy/11'' beam. Over the whole map, the noise increases with distance from the center because of the scanning law of the telescope. The color code is blue, purple, red, orange, yellow, and white for increasing positive intensity and black for all negative intensities. The pixel size is 3.5'', and the noise is uncorrelated across pixels.

In the intensity map of Fig 1, a ring is clearly apparent in the central region of the map, and a point source is located within only one pixel (3.5'') from the map center. Moreover, there are negative (black) side lobes east and west of the ring, which have slightly distorted the outer

¹ <http://www.iram.es/IRAMES/mainWiki/CookbookMopsic>

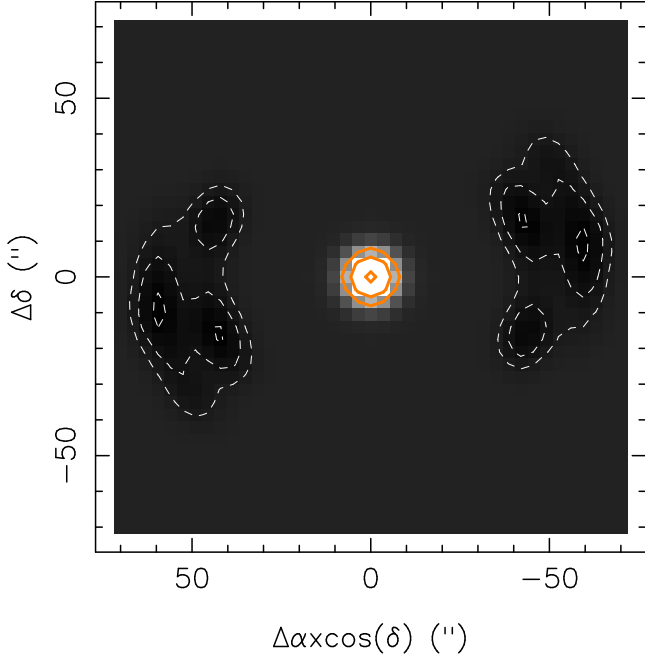


Fig. 2. Synthesized beam resulting from the shift-and-add procedure used to restore the *MAMBO* map from the chopped observations of the ϵ Eridani field conducted on nine days between November 16 and December 4, 2007. Each observation is 48 minutes long. The hour angles of the observations comprise only ± 2 hours because ϵ Eridani culminates at the relatively low elevation of 43° at Pico Veleta. Dashed white contours are -7%, -4%, -2%, orange contours are +25%, +50%, +90%, of the peak at the center.

edges of the structure. This is expected given that the observations were taken over a limited range of hour angles (± 2 hours), producing the point spread function shown in Fig. 2 for the shift-and-add procedure of image restoration. To overcome these slight systematics in the map, we restored the map with the CLEAN algorithm (Högbom 1974), which is widely used for image restoration in radio interferometry with complicated point spread functions because of limited $u-v$ coverage (Clark 1980). With this algorithm, the central region of the map of Fig. 1 was first deconvolved iteratively with the synthesized beam of Fig. 2 by adopting a gain of 0.1 (fraction of the synthesized beam scaled to the map maximum and removed at each iteration), and in running five hundred iterations that produced 46 CLEAN δ -functions. Then, these resulting CLEAN spikes were convolved with a 2D Gaussian with a FWHM of $10.7''$ for the beam of the telescope. The final CLEAN map is shown in Fig. 3, from which the photosphere has been subtracted and the residual map not added back for clarity, as is standard.

3. Photometric excess of ϵ Eridani at long wavelengths

A ring is clearly apparent in the central region of Fig. 1. Additionally, a point source is coincidental with the position of ϵ Eridani at the date of observation (map center) within astrometric uncertainty ($3.5''$). The measured flux density of this point source is 1.2 ± 0.3 mJy. This is somewhat in excess of the flux density of 0.53 ± 0.25 mJy for the photosphere of ϵ Eridani we predicted at $\lambda = 1.2$ mm with

the NexGen stellar atmospheric model (Hauschildt et al. 1999), $T_{eff} = 5034 \pm 228$ K (Paletou et al. 2015), and the UBVRIJHK magnitudes in Ducati (2002).

Greaves et al. (2014) have detected a warm component associated with ϵ Eridani in their *Herschel* PACS images that they modeled with an inner belt of 14 AU in radius ($4''$). The flux density of their model (their Fig. 3) extrapolated at 1.2 mm is higher than 5 mJy, meaning that it is well in excess of our MAMBO measurement (1.2 ± 0.3 mJy), but it may contribute to the slight excess above the photospheric level just mentioned. Their model is based on a modified blackbody law; their emission spectrum scales as $\lambda^{-(2+\beta)}$ with $\beta = 0.4$ longward of $150 \mu\text{m}$. A steeper spectrum is required with our MAMBO measurement, which indicates a population of smaller dust grains in this warm belt.

Aperture photometry made in our MAMBO image of Fig. 1 has yielded a total flux density of 17.3 ± 3.5 mJy at 1.2 mm within a radius of $30''$, including the contribution of the point source. The uncertainty includes statistical error and a 10% error in absolute flux calibration. A first map of the structure around ϵ Eridani at 1.2 mm was made with the *SIMBA* bolometer array at the *SEST* radiotelescope in Chile with a beam FWHM of $24''$. This map showed an extended structure that can be fit with a circular Gaussian intensity distribution with a FWHM of $36.4''$ and a total flux density of 21.4 ± 5.1 mJy (Schütz et al. 2004), which is consistent with our measurement at the same wavelength. An earlier millimeter observation of ϵ Eridani was conducted with an *MPIfR* bolometer system also at *SEST* and yielded 24.2 ± 3.4 mJy at $1300 \mu\text{m}$ (Chini et al. 1991), somewhat in excess of our measurement, even though we observed at a shorter wavelength.

Properties of emitting particles in the cold belt can be tested with the modified blackbody law. From the total flux density of 37.0 ± 2.5 mJy at $850 \mu\text{m}$ (Greaves et al. 2005) and our measurement at 1.2 mm, one finds $\beta = 0.4^{+0.6}_{-0.4}$. Notwithstanding the large uncertainty, this value is lower than $\beta = 1.0 \pm 0.15$ calculated between 450 and $850 \mu\text{m}$ ($S_{450} = 250 \pm 20$ mJy in Greaves et al. (2005)) and might indicate a change in slope for the emission of medium-sized particles (pebbles).

The compound of these slopes and uncertainties, however, is consistent with the model developed by Gáspár et al. (2012) for a collisional cascade that reaches equilibrium with a mass distribution that is steeper than the traditional solution by Dohnanyi. Their model implies a slope of -2.65 ($\beta = 0.65$) for the long-wavelength Rayleigh-Jeans tail of the SED, consistent with our values of β above. The slope of their model does not depend on material properties of the medium-sized particles since they predominantly contribute to the emission at long-wavelength in fully absorbing the incident light of the star ($Q_{abs} = 1$), as also discussed in Wyatt & Dent (2002).

4. Observed azimuthal structure around ϵ Eridani

The final *MAMBO* image of the structure around ϵ Eridani at 1.2 mm is presented in Fig. 3 with the photosphere subtracted. The ring-like appearance is striking and was originally discovered in *SCUBA* images at $450 \mu\text{m}$ and $850 \mu\text{m}$ (Greaves et al. 1998, 2005), the latter is reproduced in Fig. 4.

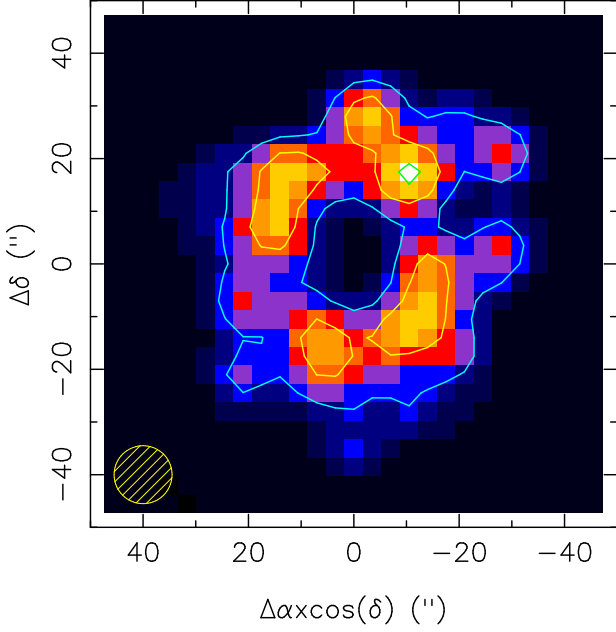


Fig. 3. *MAMBO* intensity map of the structure around ϵ Eridani at $\lambda = 1.2\text{mm}$ restored with the CLEAN algorithm. The star ϵ Eridani is at the map center (0,0), which is at $\alpha = 3^{\text{h}} 32^{\text{m}} 55.32^{\text{s}}$ and $\delta = -9^{\circ} 27' 29.7''$ (15 November 2007). The telescope beam is shown as a hatched circle (FWHM = $10.7''$). Contour levels are 30%, 60%, and 90% of the northwest brightness peak. The first contour (30%) is at the level of the CLEAN residuals, which were not added back to the map for clarity, as is standard. The point source (1.2 mJy) close to the map center has been subtracted (see text of Sect. 3).

The pixel size is $3.5''$, and the map is unsmoothed.

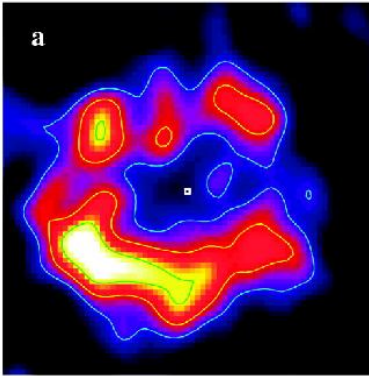


Fig. 4. *SCUBA* intensity image of the structure around ϵ Eridani observed at $\lambda = 850\ \mu\text{m}$ in Greaves et al. (2005). The full field is $70''$ wide in RA and DEC coordinates; north is up and east to the left.

The main features in the *MAMBO* and *SCUBA* images are similar. There are four emission clumps in the southeast, northeast, northwest, and southwest sectors, and there

Table 1. Coordinates of the four emission clumps in the images.

Sector	MAMBO		SCUBA	
	$\Delta\alpha\cos\delta\ (")$	$\Delta\delta\ (")$	$\Delta\alpha\cos\delta\ (")$	$\Delta\delta\ (")$
NW	-9.5	+18	-11	+16
SW	-9.5	-9	-12	-11
NE	+16	+9	+16	+11
SE	+6	-15	+18	-13

are two deep hollows to the east and west (east is toward positive RA). These features are similarly located in the two images except for the southeast clump, as reported in Table 1. This positional coincidence with the exception of the southeast clump is also apparent by comparing the *MAMBO* and *SCUBA* azimuthal profiles shown in Fig. 5.

Hence, the most noticeable difference is the southeast clump, which appears as a prominent arc-like feature in the *SCUBA* image while it is clearly more compact and fainter in the *MAMBO* image. However, in the most recent image of ϵ Eridani with *SCUBA2* (Greaves and Holland, private communication), this clump is actually point-like and positioned consistently with its counterpart in the *MAMBO* image. In fact, it is possible that the arc-like feature in the earlier *SCUBA* image is an artifact that is due to incomplete removal of atmospheric fluctuations.

The *MAMBO* structure we observed in November 2007 (Fig. 3) is slightly elongated in the north-south direction, while the *SCUBA* structure resulting from the integration of data from 1997 to 2002 (Fig. 4) is oriented southeast to northwest. This appears inconsistent, but the most recent image of ϵ Eridani made in March 2011 with *Herschel/PACS* shows a structure that is slightly elongated in the north-south direction (Greaves et al. 2014), thus similar as with *MAMBO* in November 2007. Greaves and colleagues argued that the eastwest extension seen earlier was caused by the disk moving against a background of contaminant sources, with the significant proper motion of the star ($1''/\text{yr}$) almost entirely westward (see also Poulton et al. (2006)). Hence, these contaminants contribute to the brightness distribution of the disk, and snapshots will eventually disentangle the two emissions. It is already clear from the available data, however, that the disk emission dominates.

The slight elongation of the structure in the north-south direction is indicative of a moderately inclined structure (32°) (Greaves et al. 2014).

The overall agreement between the two images made with *MAMBO* and *SCUBA* provides tentative evidence of the presence of four emission clumps, but to characterize them fully, additional observations are required.

5. Observed radial structure around ϵ Eridani

The radial brightness profile of the structure in Fig. 6 was calculated by averaging intensities over $4''$ wide, elliptical annuli of increasing radii. To maximize the peak of the profile, the structure must be projected on the sky with an inclination of $\sim 25^\circ$ and PA of $\sim 0^\circ$, and the center of the ellipses must be displaced by $2''$ westward from the map center. This optimal geometry is consistent with the slightly inclined structure (32°) along the north-south direction

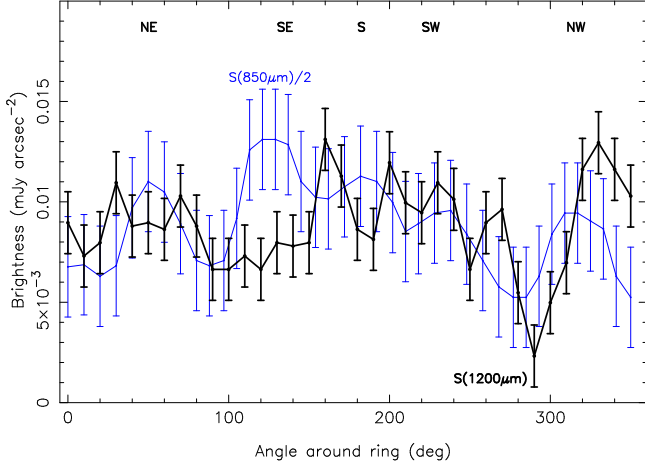


Fig. 5. Azimuthal profiles of the dust emission around ϵ Eridani computed for *MAMBO* (black) and *SCUBA* (blue). The *MAMBO* profile has been computed from the unsmoothed image with the photosphere subtracted. Each *MAMBO* point represents the mean brightness over a small sector with an opening angle of 10° and ranging radially from $10''$ to $30''$. Points are independent and uncertainties are the noise rms of the map divided by the square root of the number of pixels in each sector (~ 6 pixels). The *SCUBA* profile is from Greaves et al. (2005) and has been divided by 2, for clarity. The SE counterpart is inconsistent between *MAMBO* and *SCUBA*; this is discussed in Sect. 4. The angle increases counterclockwise from zero at north, and clumps are labeled.

seen in the $160 \mu\text{m}$ image provided with *Herschel*/PACS (Greaves et al. 2014).

We have fit a Gaussian and a constant level ($c + a \exp(-0.5 \times ((r - r_0)/\sigma_0)^2)$) to this measured radial profile and found a constant level $c = -0.08 \pm 0.03 \text{ mJy}/11''\text{beam}$, an amplitude $a = 1.65 \pm 0.13 \text{ mJy}/11''\text{beam}$, a peak radius $r_0 = 17.7 \pm 0.4''$, and an FWHM $= 2\sigma_0 \times \sqrt{2 \ln 2} = 12 \pm 1''$. The fit is characterized by a normalized χ^2_ν of 0.95 for the number of degrees of freedom of 26. The peak radius ($17.7'' \pm 0.4''$) is comparable to $\sim 18''$ measured in Greaves et al. (2005).

Hence, at the distance of the star of 3.2 pc, this peak radius corresponds to $R = 57 \pm 1.3 \text{ AU}$. The fit FWHM of the profile is consistent with the *IRAM* 30-meter radiotelescope beam of $10.7''$ (Kramers et al. 2013). Thus, we estimated limits for the belt width ΔR in deconvolving the profile with the measured lower and upper limits of its FWHM, $11'' \leq \sqrt{10.7''^2 + (\Delta R)^2} \leq 13''$, and found $2.5'' \leq \Delta R \leq 7''$, or $8 \leq \Delta R \leq 22 \text{ AU}$ at 3.2 pc. Hence, the fractional belt width is $0.1 \leq \Delta R/R \leq 0.4$, smaller than the fractional width of the Kuiper Belt $\Delta R/R$ of 0.5 in Stern & Colwell (1997), and possibly as narrow as the belt around Fomalhaut at millimeter wavelength (Boyles et al 2012).

Our upper limit of the width of the belt around ϵ Eridani is more stringent than the estimate made from the radial profile at $850 \mu\text{m}$ in Greaves et al. (2005) because the beam of the JCMT is broader ($14''$). Moreover, Greaves et al. (2014) modeled their *Herschel* PACS images and determined a mean radius of 61 AU and a width of $\sim 15 \text{ AU}$

($\Delta R/R = 0.2 - 0.3$), indicating that the belt is quite radially confined according to the model.

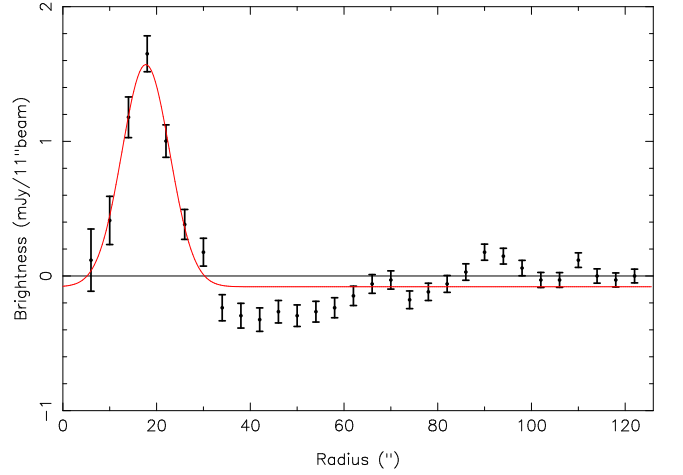


Fig. 6. Radial profile of the dust emission around ϵ Eridani computed from the photosphere-subtracted *MAMBO* image. Points are independent and represent the mean brightness calculated over $4''$ wide, elliptical annuli of increasing semi-major axis (structure is inclined by 25° relative to the plane of the sky along the north-south direction ($\text{PA}=0^\circ$)). The uncertainty of each brightness point is the noise rms of the map divided by the square root of the number of pixels in each annulus. The Gaussian in red is based on the four-parameter fit described in Sect. 5.

6. Discussion

6.1. Robustness of the clumps in the *MAMBO* and *SCUBA* images

Asymmetries and clumps observed in images of debris disks can be related, in theory, to dust and planetesimals trapped in resonances with planets just interior to the inner edge of the belt (e.g. Liou et al. 1996; Ozernoy et al. 2000; Wyatt 2003; Krivov et al. 2007). However, reliable identification of predicted structures in real images at long wavelength has been difficult. For example, Piétu et al. (2011) and Hughes et al. (2012) could not recover the clumpy structure around Vega reported earlier. Similarly, Hughes et al. (2012) could not confirm the asymmetries found above 3σ in the structure around HD 107146 in previous observations.

In contrast, for ϵ Eridani, the similarities between the *MAMBO* and *SCUBA* images discussed here provide tentative evidence that the observed structure is robust. The four clumps may result from mean-motion resonances with an unseen planet in the system that is not detectable with current radial velocity measurements because its orbital period is as long as tens or hundreds of years.

Inferring the orbital parameters of a planet from its imprint on the structure of a disk is an area of active research. The ring-like structure of the solar system between 30 and 50 AU has been described as particles trapped in mean-motion resonances with Neptune, and the clearing within 10 AU described as particles ejected because of the giant planets Jupiter and Saturn (Liou et al. 1996; Liou & Zook 1999; Moro-Martín & Malhotra 2002).

Table 2. Sizes of debris disks estimated from images at long wavelength.

		R_{in} (AU)	R_{out} (AU)	R_{mean} (AU)	ΔR (AU)	$\Delta R/R_{mean}$	λ (μm)		ref.
Vega	A0V	< 85	> 105			> 0.2	1300	IRAM-PdB	1
HD21997	A3IV/V	55 ± 16			< 108 ^a	< 2	886	ALMA	2
Fomalhaut	A4V			141.5	16 ± 3	0.1	857	ALMA	3
HD107146	G2V	50	170			1.1	880	ALMA	4
η Corvi	F2V			164 ± 4	< 60	< 0.3	850	SCUBA2	5
Sun	G2V	30	50			0.5		—	6
ϵ Eridani	K2V			57 ± 1.3	< 22	< 0.4	1200	IRAM-30m	7
AU Mic	M1V	8^{+11}_{-1}	40 ± 0.4			1.3	1300	ALMA	8

References. (1) Piétu et al. (2011); (2) Moór et al. (2013); (3) Boley et al. (2012); (4) Hughes et al. (2011); (5) Duchêne et al. (2014); (6) Stern & Colwell (1997); (7) this work; (8) MacGregor et al. (2013).

Notes. ^a angular resolution is $1.5''$, the belt is smaller than beam, hence $\Delta R < 1.5'' \times 72 \text{ pc} = 108 \text{ AU}$.

Clumps due to mean-motion resonances must be significantly enhanced to be observable, and two mechanisms have been studied. Dust grains can be trapped into resonances during their transport inward by Poynting-Robertson drag (Roques et al. 1994; Kuchner & Holman 2003; Deller & Maddison 2005), or resonant planetesimals and grains can be swept along during planet migration (Wyatt 2003; Reche et al. 2008). First-order mean-motion resonances ($p + 1 : p$, $p > 0$) with low p are the strongest, but planet mass and orbit eccentricity have a significant impact on the final structure (Reche et al. 2008).

Predicting the number of observable clumps and their relative intensities requires additional constraints. Marengo et al. (2009) determined an upper limit of four Jupiter masses for any planet (1 Gyr models) inside the inner rim of the submillimeter ring of ϵ Eridani with *Spitzer/IRAC* data. We note also that the two hollows east and west seen consistently in both the *SCUBA* and *MAMBO* images require a planet of sub-Jupiter mass if arising from first-order mean-motion resonances according to several simulations (Ozernoy et al. 2000; Quillen & Thorndike 2002; Reche et al. 2008).

6.2. Narrow belt of planetesimals around ϵ Eridani

The *MAMBO* image in Fig. 3 and the radial brightness profile in Fig. 6 currently provide the most stringent upper limit on the width of the planetesimal belt around ϵ Eridani determined directly from observations. In Table 2, we compare this relative width ($0.1 \leq \Delta R/R \leq 0.4$) to the sizes of debris disks determined from millimeter or submillimeter observations that trace parent planetesimals. Given its mean radius of $57 \pm 1.3 \text{ AU}$, the belt around ϵ Eridani has a cavity of a few tens of AU, which can host a large planetary system.

The inner edge of a planetesimal belt results from the planetary formation phase when the largest planets eject smaller bodies into the Oort cloud (Goldreich et al. 2004), and from outward migration (Levison & Morbidelli 2003). The outer edge is set by the competition between viscous spreading in the protoplanetary disk and disruptive effect of stellar flybys in star forming region (Rosotti et al. 2014). Additionally, at a later stage of evolution, the outer edge of the disk can be truncated further and its mass depleted as a result of other destructive stellar flybys for a period

as long as $\sim 100 \text{ Myr}$, when the central star is still in the expanding open cluster of its birth (Lestrade et al. 2011).

The belt around ϵ Eridani (57 AU , $0.1 \leq \Delta R/R \leq 0.4$) is narrower and at a larger distance than the present-day Kuiper Belt ($R_{mean} = 40 \text{ AU}$, $\Delta R/R = 0.5$) (Stern & Colwell 1997, inner edge $\sim 30 \text{ AU}$ and outer edge $\sim 50 \text{ AU}$). Furthermore, planetesimals most probably formed within $\sim 30 \text{ AU}$ in the solar system and were subsequently pushed outward by Neptune’s 2:1 mean-motion resonance during its final phase of migration. This means that the entire Kuiper Belt formed closer to the Sun and was transported outward during the final stages of planet formation (Levison & Morbidelli 2003). Hence, the original Kuiper Belt around the younger Sun was more compact than it is today, contrasting even more with the relatively large belt around ϵ Eridani, which is only 850 Myr in age (Di Folco et al. 2004).

It is useful to compare the properties of the disk around ϵ Eridani also with other disks that are spatially resolved and are listed in Table 2. The broadest belt is around the solar-type star HD107146 with $\Delta R/R \sim 1.1$ (Hughes et al. 2011, inner radius $\sim 50 \text{ AU}$, outer radius $\sim 170 \text{ AU}$), and the narrowest belt is around the A-type star Fomalhaut A with $\Delta R/R \sim 0.1$ (Boley et al. 2012, mean radius 135 AU , width $16 \pm 3 \text{ AU}$). These authors also showed that two shepherding planets on both sides of the belt of Fomalhaut A can be responsible for its narrow width. This might be of interest for the ϵ Eridani belt.

Finally, our characterization of the belt around ϵ Eridani with a mean radius of $57 \pm 1.3 \text{ AU}$ and a width smaller than $< 22 \text{ AU}$ is not consistent with model fits to the SED of this star. Backman et al. (2009) found a broader submillimeter ring between 35 and 90 AU , and Reidemeister et al. (2011) found a birth ring between 55 to 90 AU . In this latter model dust grains are transported inward by Poynting-Robertson and stellar wind drags and are constrained by the $850 \mu\text{m}$ flux density from JCMT/SCUBA. Unfortunately, the authors of these two studies did not predict the flux density of the disk at 1.2 mm for comparison with our *MAMBO* measurement.

7. Conclusion

The *MAMBO* image of the debris disk around ϵ Eridani at 1.2 mm we presented shows a structure similar to the one identified earlier with *SCUBA* at 850 μm : a ring-like structure broken into four emission clumps in the northeast, northwest, southwest, southeast sectors, and two deep hollows east and west. In theory, this structure can be the imprint of resonant clumps related to gravitational perturbations from undetected long-period planets in the system.

However, the reliability of images made with a single radiotelescope and bolometer camera has been debated before because these images can be distorted if the signal of the large atmospheric fluctuations inherent in this type of observation is not completely removed from the data.

We argued that the identification of three of the four emission clumps (NE, NW, SW) at the same locations within astrometric uncertainty in two images made with different radiotelescopes, namely the *IRAM* 30-meter and *JCMT*, and different bolometer cameras, namely *MAMBO* and *SCUBA*, provides tentative evidence that the observed structure is robust. The southeast clump is the most discrepant in brightness and extension in the two images, but it is possible that this is an artifact. Overall, this provides new impetus for future studies to relate this structure to the presence of undetected planets in the system.

Additionally, we provided the most stringent upper limit on the width of the belt of planetesimals around ϵ Eridani with $8 \leq \Delta R \leq 22$ AU. This corresponds to a relative width of $0.1 \leq \Delta R/R \leq 0.4$, which is narrower than for the Kuiper Belt.

Future observations at long wavelengths on finer scales with interferometers will provide additional information on the emission clumps in the belt around ϵ Eridani, for instance, their true size, to investigate the interplay between debris disks and associated planetary systems.

Acknowledgements. We are grateful to the staff of the IRAM 30-m telescope, especially Stéphane Leon now at ALMA, for his dedication in managing the MAMBO pool, to Patrick Charlot at Observatoire de Bordeaux for useful discussions on the CLEAN algorithm, and to Sarah Maddison at Swinburne University for her benevolent assistance. We are very grateful to our referee for constructive suggestions that have improved the paper. This work was funded in part by CNES and CNRS PNP.

References

- Anglada-Escudé, G. & Butler, R. P. 2012, *ApJS*, 200, 15
 Augereau, J.-C. & Beust, H. 2006, *A&A*, 455, 987
 Aumann, H. H. 1988, *AJ*, 96, 1415
 Backman, D., Marengo, M., Stapelfeldt, K., et al. 2009, *ApJ*, 690, 1522
 Benedict, G. F., McArthur, B. E., Gatewood, G., et al. 2006, *The Astronomical Journal*, 132, 2206
 Boley, A. C., Payne, M. J., Corder, S., et al. 2012, *ApJ*, 750, L21
 Chini, R., Kruegel, E., Kreysa, E., Shustov, B., & Tutukov, A. 1991, *A&A*, 252, 220
 Clark, B. G. 1980, *A&A*, 89, 377
 Cumming, A., Marcy, G. W., & Butler, R. P. 1999, *The Astrophysical Journal*, 526, 890
 Deller, A. T. & Maddison, S. T. 2005, *ApJ*, 625, 398
 Di Folco, E., Thévenin, F., Kervella, P., et al. 2004, *A&A*, 426, 601
 Ducati, J. R. 2002, *VizieR Online Data Catalog*, 2237, 0
 Duchêne, G., Arriaga, P., Wyatt, M., et al. 2014, *ApJ*, 784, 148
 Emerson, D. T., Klein, U., & Haslam, C. G. T. 1979, *A&A*, 76, 92
 Gáspár, A., Psaltis, D., Rieke, G. H., & Özel, F. 2012, *ApJ*, 754, 74
 Gillett, F. C. 1986, in *Astrophysics and Space Science Library*, Vol. 124, *Light on Dark Matter*, ed. F. P. Israel, 61–69
 Goldreich, P., Lithwick, Y., & Sari, R. 2004, *ApJ*, 614, 497
 Greaves, J. S., Holland, W. S., Moriarty-Schieven, G., et al. 1998, *ApJ*, 506, L133
 Greaves, J. S., Holland, W. S., Wyatt, M. C., et al. 2005, *ApJ*, 619, L187
 Greaves, J. S., Sibthorpe, B., Acke, B., et al. 2014, *ApJ*, 791, L11
 Hatzes, A. P., Cochran, W. D., McArthur, B., et al. 2000, *The Astrophysical Journal Letters*, 544, L145
 Hauschildt, P. H., Allard, F., Ferguson, J., Baron, E., & Alexander, D. R. 1999, *ApJ*, 525, 871
 Högbom, J. A. 1974, *A&AS*, 15, 417
 Hughes, A. M., Wilner, D. J., Andrews, S. M., et al. 2011, *ApJ*, 740, 38
 Hughes, A. M., Wilner, D. J., Mason, B., et al. 2012, *ApJ*, 750, 82
 Kral, Q., Thebault, P., Augereau, J.-C., Boccaletti, A., & Charnoz, S. 2014, *ArXiv e-prints*
 Kramers, C., Peñalver, J., & Greve, A. 2013, *Improvement of the IRAM 30m Telescope Beam Pattern*, IRAM: Memo 26 August 2013, Version 8.2
 Kreysa, E., Gemuend, H.-P., Gromke, J., et al. 1998, in *Society of Photo-Optical Instrumentation Engineers (SPIE) Conference Series*, Vol. 3357, *Advanced Technology MMW, Radio, and Terahertz Telescopes*, ed. T. G. Phillips, 319–325
 Krivov, A. V., Queck, M., Löhne, T., & Sremčević, M. 2007, *A&A*, 462, 199
 Kuchner, M. J. & Holman, M. J. 2003, *ApJ*, 588, 1110
 Lestrade, J.-F., Morey, E., Lassus, A., & Phou, N. 2011, *A&A*, 532, A120
 Levison, H. F. & Morbidelli, A. 2003, *Nature*, 426, 419
 Liou, J.-C. & Zook, H. A. 1999, *AJ*, 118, 580
 Liou, J.-C., Zook, H. A., & Dermott, S. F. 1996, *Icarus*, 124, 429
 MacGregor, M. A., Wilner, D. J., Rosenfeld, K. A., et al. 2013, *ApJ*, 762, L21
 Marengo, M., Stapelfeldt, K., Werner, M. W., et al. 2009, *ApJ*, 700, 1647
 Matthews, B. C., Krivov, A. V., Wyatt, M. C., Bryden, G., & Eiroa, C. 2014, *ArXiv e-prints*
 Metcalfe, T. S., Buccino, A. P., Brown, B. P., et al. 2013, *ApJ*, 763, L26
 Moór, A., Juhász, A., Kóspál, Á., et al. 2013, *ApJ*, 777, L25
 Moro-Martín, A. & Malhotra, R. 2002, *AJ*, 124, 2305
 Ozernoy, L. M., Gorkavyi, N. N., Mather, J. C., & Taidakova, T. A. 2000, *ApJ*, 537, L147
 Paletou, F., Böhm, T., Watson, V., & Trouillet, J.-F. 2015, *A&A*, 573, A67
 Piétu, V., di Folco, E., Guilloteau, S., Gueth, F., & Cox, P. 2011, *A&A*, 531, L2
 Poulton, C. J., Greaves, J. S., & Collier Cameron, A. 2006, *MNRAS*, 372, 53
 Quillen, A. C. & Thorndike, S. 2002, *ApJ*, 578, L149
 Reche, R., Beust, H., Augereau, J.-C., & Absil, O. 2008, *A&A*, 480, 551
 Reidemeister, M., Krivov, A. V., Stark, C. C., et al. 2011, *A&A*, 527, A57
 Roques, F., Scholl, H., Sicardy, B., & Smith, B. A. 1994, *Icarus*, 108, 37
 Rosotti, G. P., Dale, J. E., de Juan Ovelar, M., et al. 2014, *ArXiv e-prints*
 Schütz, O., Nielbock, M., Wolf, S., Henning, T., & Els, S. 2004, *A&A*, 414, L9
 Stern, S. A. & Colwell, J. E. 1997, *ApJ*, 490, 879
 Thebault, P., Kral, Q., & Augereau, J.-C. 2014, *A&A*, 561, A16
 Wyatt, M. C. 2003, *ApJ*, 598, 1321
 Wyatt, M. C. 2008, *ARA&A*, 46, 339
 Wyatt, M. C. & Dent, W. R. F. 2002, *MNRAS*, 334, 589
 Wyatt, M. C., Dermott, S. F., Telesco, C. M., et al. 1999, *ApJ*, 527, 918